Narrow-Band Microwave Filter Design

Daniel G. Swanson, Jr.

As early as 1951, Dishal [1] recognized that any narrow-band, lumped-element, or distributed bandpass filter could be described by three fundamental variables: the synchronous tuning frequency of each resonator, f_0; the couplings between adjacent resonators, $K_{r,r+1}$; and the singly loaded or external Q of the first and last resonators, Q_{ex}. He also demonstrated that filter hardware could be tuned or aligned using knowledge of these fundamental parameters. For purposes of this discussion, "narrow band" is defined to be up to 10% relative bandwidth and perhaps as high as 20% relative bandwidth.

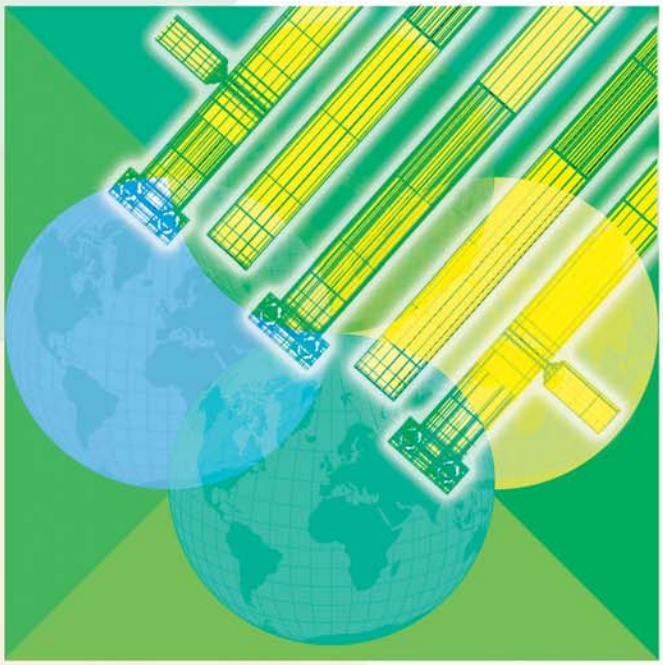

© ARTVILLE

In a later paper, Dishal [2] outlined a design procedure for tapped interdigital filters using the f_0, $K_{r,r+1}$, and Q_{ex} parameters. Once the required Ks and Q_{ex}s are known, Dishal's method uses measured experimental hardware to generate a design curve for each parameter. Almost 15 years later, after microstrip technology became more popular, Wong [3] demonstrated how Dishal's method could be applied to the design of microstrip distributed filters with tapped inputs and outputs. Again, experimental data was used to generate design curves for coupling between resonators and external Q.

Before electromagnetic (EM) field solvers became widely available, generating these two design curves required a rather tedious process of measuring, modifying, and remeasuring a set of experimental hardware. In the last few years, it has become more common to generate coupling and external Q curves using data from an EM field solver. Puglia [4], [5] and Rhea [6] have published excellent tutorials on combining Dishal's concepts with EM simulation. Hong and Lancaster [7] also present examples of how these concepts can be applied

Daniel G. Swanson, Jr. is with Tyco Electronics, Lowell, MA.

Digital Object Identifier 10.1109/MMM.2007.904724

TABLE 1. Chebyshev lowpass prototype.

.036-dB Ripple, 20.8 dB Return Loss, 1.20 VSWR

N	g_0	g_1	g_2	g_3	g_4	g_5	g_6	g_7	g_8	g_9	g_{10}	$\sum_{i=1}^{N} g_i$
2	1.0000	0.6323	0.5269	1.1999								1.1592
3	1.0000	0.8185	1.0895	0.8185	1.0000							2.7265
4	1.0000	0.8989	1.2843	1.5410	0.7491	1.1999						4.4733
5	1.0000	0.9393	1.3677	1.7691	1.3677	0.9393	1.0000					6.3831
6	1.0000	0.9622	1.4104	1.8636	1.5531	1.6924	0.8019	1.1999				8.2836
7	1.0000	0.9763	1.4353	1.9115	1.6278	1.9115	1.4353	0.9763	1.0000			10.2739
8	1.0000	0.9857	1.4509	1.9392	1.6650	1.9979	1.6162	1.7410	0.8215	1.1999		12.2173
9	1.0000	0.9921	1.4615	1.9568	1.6864	2.0403	1.6864	1.9568	1.4615	0.9921	1.0000	14.2340

to several different planar filter topologies. The discussion of coupling concepts for planar filters in [7] is the most complete one currently available.

In this article, we will combine Dishal's concepts, EM simulation, and the port-tuning concept [8], [9] to outline a very general and powerful procedure for narrow-band filter design. When applied to an EM-based filter prototype, port tuning gives a direct indication of the magnitude and direction of the tunings needed to correct coupling errors and resonator frequency errors. An EM-based filter prototype potentially captures all the physics of the real hardware and includes second-order effects that may be impossible to describe using analytical models. After iteratively reducing all the errors in the EM-based prototype, we can be confident that the first hardware prototype that we build will meet our performance goals. This design methodology can be applied to simple all-pole Chebyshev filters and to more complex cross-coupled filters that place transmission zeros in the stopbands.

Dishal's Method

A bandpass filter specification generally includes the desired center frequency, percentage bandwidth, maximum insertion loss in the passband, and several required rejection levels in the stopbands. There will also be a specification on the minimum return loss in the passband. A return loss of 26.4 dB (1.10 VSWR) corresponds to a prototype ripple level of .01 dB. A return loss of 20.8 dB (1.20 VSWR) corresponds to a prototype ripple level of .036 dB. Many mechanical filters with tuning screws can eventually be tuned to their designed return loss level. In printed filters, which are much harder to tune, we might design for 20-dB return loss and hope that we achieve a minimum of 15 dB in practice. At the system level, we would like to have components with a minimum return loss around 15 dB to avoid mismatch ripple when components are cascaded.

Once the prototype ripple level has been determined, the filter order N can be estimated based on the desired stopband rejection. The graphs and equations in Matthaei, Young, and Jones [10] are very useful for estimating filter order. Note that the graphs and equations assume an ideal, symmetrical Chebyshev response. Very few microwave filters have symmetrical stopband responses, so the required order may be higher or lower than what we originally estimate. With the ripple level and order N determined, we can go to the tables or equations for the normalized lowpass prototype values. Table 1 lists the normalized element values for a .036-dB ripple, Chebyshev lowpass prototype.

At this point, we can estimate the midband filter loss using the expected average unloaded Q for the resonators

$$Loss(f_0) = \frac{4.343 f_0}{\Delta f Q_u} \sum_{i=1}^{N} g_i \text{ (dB)}, \tag{1}$$

where Δf is the equal ripple bandwidth of the filter and the sum of the g_is can be found in the last column of Table 1. Equation (1) can also be rearranged to predict the required unloaded Q given a desired midband insertion loss. Unloaded Q is proportional to a dominant resonator dimension and can be sensitive to manufacturing processes as well. Filter designers often feel most comfortable using performance data from previous designs to estimate the available Q_u for a current design project. Insertion loss in the passband is also proportional to time delay and will increase at the band edges. Weinberg [11] gives an equation for Chebyshev time delay which can be used to estimate insertion loss across the passband.

When we are confident that the chosen prototype values and the available Q_u will meet our design goals, we can derive the required Ks and Q_{ex}s from a few very simple equations

$$K_{i,i+1} = \frac{BW}{\sqrt{g_i \cdot g_{i+1}}} \text{ for } i = 1 \text{ to } (N-1), \tag{2}$$

$$Qex_1 = \frac{g_0 \cdot g_1}{BW}, \tag{3}$$

$$Qex_N = \frac{g_N \cdot g_{N+1}}{BW}, \tag{4}$$

where BW is the filter equal ripple fractional bandwidth

$$BW = \frac{\Delta f}{f_0} = \frac{f_{\text{upper}} - f_{\text{lower}}}{f_0}. \quad (5)$$

Once the required Ks and Q_{ex}s are known, Dishal's original method uses measured experimental hardware to generate two design curves. The first design curve is for coupling as a function of distance between two resonators that are tuned to the center frequency of the filter. The coupling curve might also relate some iris dimension to the coupling between resonators that are a fixed distance apart. To save space, narrowband filters often use tapped input and output resonators. The second design curve maps external Q to the position of the tap on the resonator. Once these design curves are available for a particular topology, it is a simple matter to map the desired Ks and Q_{ex}s to physical dimensions. Often some adjustment of dimensions is required in the filter prototype. Dishal's concepts can then be used to extract the realized Ks and Q_{ex}s from the prototype hardware as a guide for tuning or modification.

In the following example, we will build all the required two-resonator and single-resonator models in an EM field solver. With port tuning, it will also be obvious how to extract realized Ks and Q_{ex}s from the EM-based filter prototype.

Design Example—Microstrip Interdigital Filter

We have chosen a microstrip interdigital filter to demonstrate the design flow presented here. Among planar microwave filters, this is a popular topology due to its compact size, which is roughly $\lambda/4$ by $\lambda/4$ guide wavelengths for an $N = 5$ filter. Although the topology looks simple, a microstrip interdigital filter is actually a quite complex design problem [12]. Sophisticated two-dimensional (2-D) multistrip models exist for microstrip [13], [14], but they do not include all the housing effects. There are couplings from the filter to evanescent modes in the housing [15] that cause a significant shift in the realized bandwidth of the filter if they are not accounted for in the design. Finally, in the finished circuit, there is a very limited amount of tuning that can done to correct errors in design or manufacturing.

In the last few years, it has become more common to generate coupling and external Q curves using data from an EM field solver.

We have arbitrarily chosen an $N = 5$ filter, centered at 2.44 GHz, with a 10% band-width for this example. The lowpass prototype ripple level is .036 dB (20.8 dB return loss). No specific insertion loss or stopband rejection goals were set for this design. Using Table 1 and (2)–(5), we find $K_{1,2} = 0.0882$, $K_{2,3} = 0.0643$, and $Q_{ex} = 9.39$. To predict what insertion loss we might achieve, we need to compute Q_u for several microstrip resonators. Figure 1 shows a quarter-wavelength microstrip resonator on a 25-mil thick alumina substrate with an assumed $\varepsilon_r = 9.8$. The resonator dimensions are 50 mil by 435 mil. There are two 13-mil diameter solid metal vias to ground at the base of the resonator. There is a vent pattern around the top surface of the via that allows for outgassing during fabrication. In Sonnet *em* [16], we approximate the round vias with a 12-sided cylinder. The via region can be seen in more detail in Figure 15.

We loosely couple to the resonator with open-circuit transmission lines and adjust the coupling until $|S_{21}|$ at resonance is roughly -30 dB to -40 dB. The coupling depends on the gap between the probes and the resonator and the position of the probes along the resonator. If we measure the time delay at resonance, we can estimate the unloaded Q using

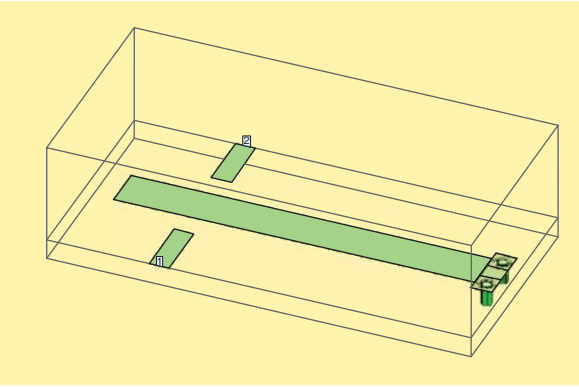

Figure 1. *Quarter-wavelength microstrip resonator on 25-mil thick alumina, $\varepsilon_r = 9.8$. The resonator dimensions are 50 by 435 mil. The two vias to ground are 13 mil in diameter. The simulation box size is 512 mil long by 256 mil wide by 150 mil high. Sonnet* em *Ver. 11.52.*

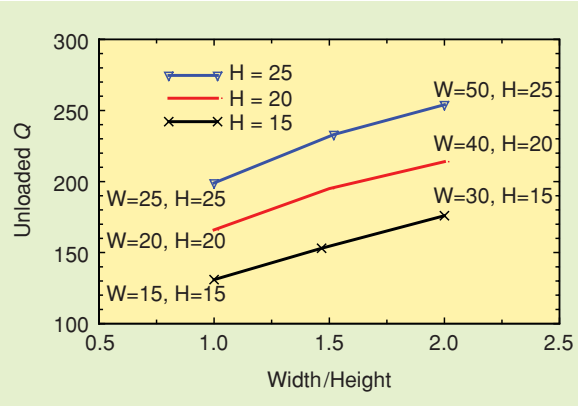

Figure 2. *Unloaded Q as a function of microstrip width over height ratio for alumina substrates at 2.44 GHz. Each curve is for a constant substrate thickness. A wide strip on a thick substrate maximizes unloaded Q. Units are mil.*

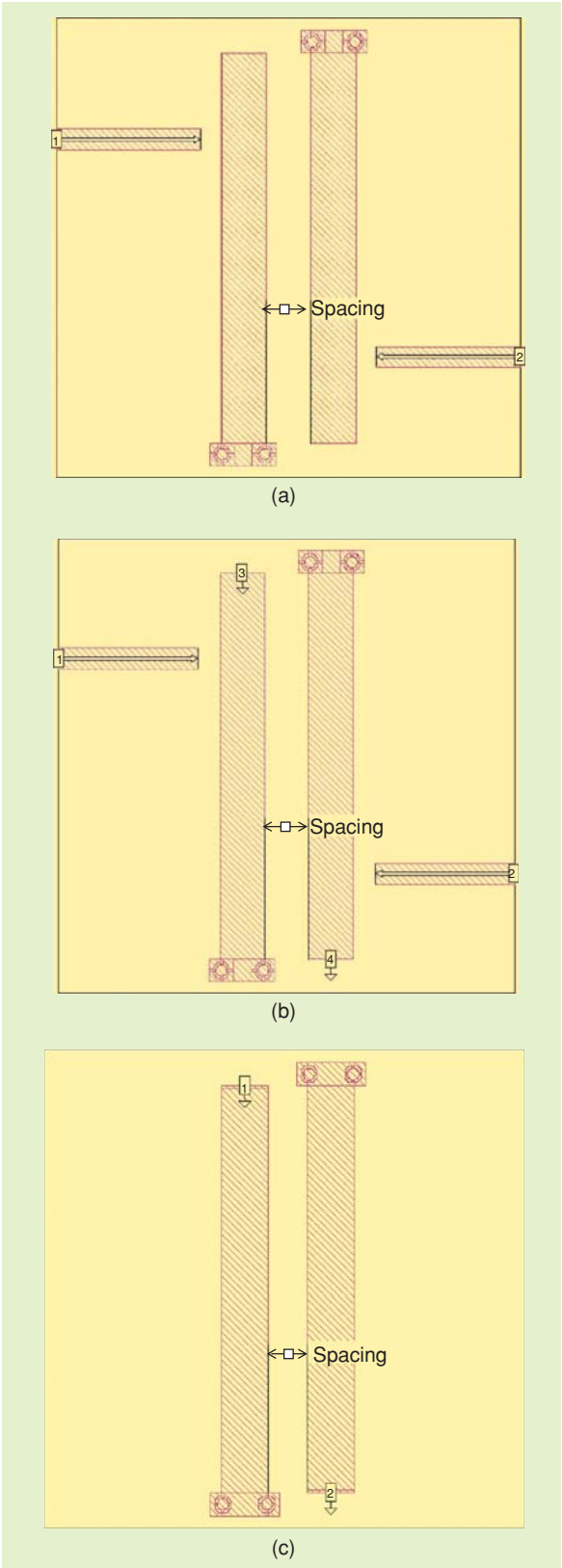

Figure 3. *(a) Two-port project with loose coupling to resonators. (b) Four-port project with autogrounded ports added for port tuning the resonators. (c) Two-port project with autogrounded ports for tuning and coupling. The simulation box size is 512 by 512 by 150 mil. Sonnet* em *Ver. 11.52.*

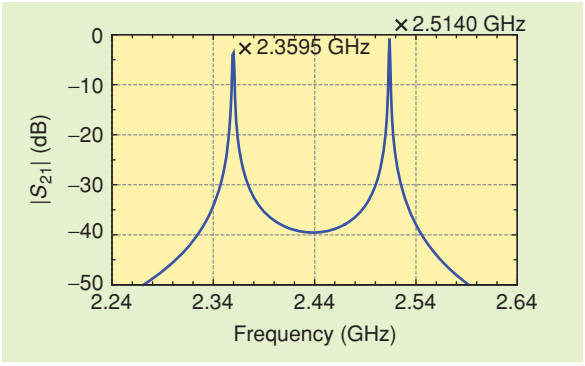

Figure 4. *Two-port insertion loss response for two loosely coupled, synchronously tuned resonators. The center frequency is 2.44 GHz. In this case, $K = 0.0633$.*

$$Q_u = \pi f_0 t_d \frac{10^{IL(dB)/20}}{10^{IL(dB)/20} - 1}. \tag{6}$$

We can run several quick experiments using the EM simulator to explore the impact of strip width and substrate thickness on unloaded Q. The results of these experiments are shown in Figure 2.

Unloaded Q was computed for three commonly used alumina substrate thicknesses and for three strip widths on each substrate. We would expect strip width and substrate thickness to both play a role, but substrate thickness is the more dominant variable. A wide strip on a thick substrate maximizes the unloaded Q. The predicted Q_u for the 50-mil wide resonator on a 25-mil substrate is 254. Equation (1) predicts a midband loss of 1.09 dB for our filter.

With the resonator geometry fixed and the desired Ks and Q_{ex} known, we can build the required design curves. Figure 3 shows three possible geometries for extracting coupling coefficients from the EM field solver.

Similar to the single-resonator case, if we loosely couple to a pair of resonators tuned to the same frequency, we get the double peak response shown in Figure 4. The null between the two peaks should be at −30 dB to −40 dB to guarantee loose coupling. The synchronous tuning condition occurs when the peaks are as close together as possible and/or when the null between the peaks is as deep as possible. The expression for the coupling coefficient is then

$$K = \frac{f_{\text{high}} - f_{\text{low}}}{f_0} = \frac{f_{\text{high}}^2 - f_{\text{low}}^2}{f_{\text{high}}^2 + f_{\text{low}}^2}, \tag{7}$$

where f_{high} is the frequency of the upper peak and f_{low} is the frequency of the lower peak.

In Figure 3(a), we have two resonators loosely coupled to input and output probes. In this case, we assume the field solver will compute the same resonant frequency for both resonators. To get a smooth $|S_{21}|$ curve, we will have to compute many discreet frequencies or have the field solver fit a response to four or five

solved frequencies. In Figure 3(b), we have added ports to ground at the resonator open ends. In the field solver, this configuration is not actually resonant. We can take the resulting four-port data and add tuning capacitors to the resonators in any circuit simulator. Because the field solver problem is not resonant, we only have to compute three frequencies around f_0 in the EM domain and can then interpolate between them in the circuit simulator. Finally, in Figure 3(c), we have removed the input and output coupling structures. When we import the two-port data to our circuit simulator, we can add tuning capacitors and lightly couple to the resonator open ends using small capacitors or transformers. Like the previous case, we only need field solver data for three frequencies in the vicinity of the filter center frequency.

We can quickly run three or four projects with different resonator spacings on the field solver and extract the coupling coefficient for each of them. If we then do a least-squares fit to a second-order polynomial function, the result is the design curve shown in Figure 5.

The fitted curve should pass through the data points with very low residual error. If the computed points cannot be fit to a low-order polynomial, the simulation method and the data extraction process should be checked for errors.

The same general procedure can now be used to generate the Q_{ex} design curve. In the field solver, we generate a project with a single resonator and tapped input/output line. If we include an extra port to ground at the open end of the resonator, we can tune the resonator to the filter center frequency in our circuit simulator, shown in Figure 6.

The tapped input line is tapered where it meets the resonator. We have found experimentally that this works better than a full-width tap line. If we measure the reflected time delay at the tap point, we can compute

$$Q_{ex} = \frac{\pi f_0 t_d}{2}, \tag{8}$$

where f_0 is in GHz and t_d is the reflected delay in ns. After setting up and solving several projects with different tap heights, we can extract the Q_{ex} data and curve-fit the results to a low-order polynomial, as shown in Figure 7.

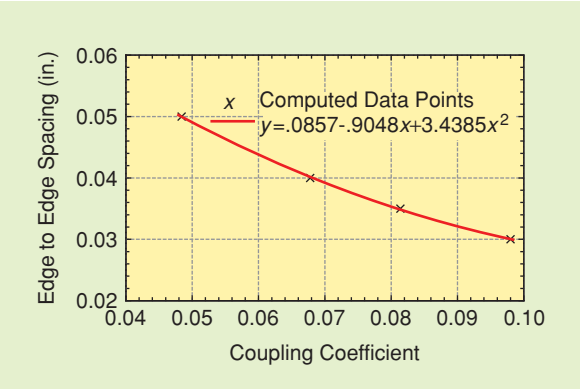

Figure 5. *Edge-to-edge resonator spacing versus coupling coefficient for the geometry shown in Figure 3.*

We combine Dishal's concepts, EM simulation, and the port-tuning concept [8], [9] to outline a very general and powerful procedure for narrow-band filter design.

By inspection and by examining the polynomial coefficients, we can see that the fitted curve is almost linear. Again, if a computed data point does not lie on the curve, it is suspect and should be recomputed.

We are now ready to build our first complete filter model in the field solver. We will choose a 1-mil grid in Sonnet *em*, which is a good compromise between geometrical resolution and solution time. Using Figure 5, $K_{1,2} = .0882$ implies a spacing of 32.6 mil, which we will round up to 33 mil. $K_{2,3} = .0643$ implies a spacing of 41.7 mil, which we will round up to 42 mil. Using Figure 7, $Q_{ex} = 9.39$ implies a tap point of 95 mil. Figure 8 shows the layout and computed results for this first iteration.

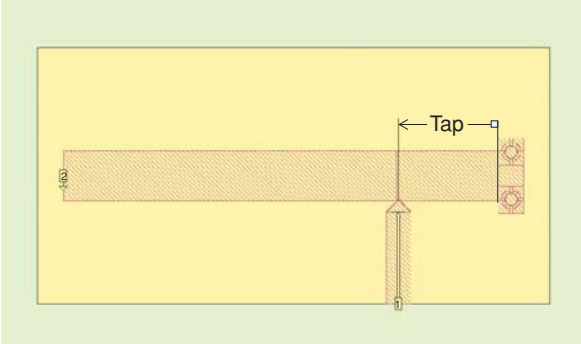

Figure 6. *Tapped resonator for computation of external Q. Note the taper in the tap line where it meets the resonator. The simulation box size is 512 by 256 by 150 mil. Sonnet* em *Ver. 11.52.*

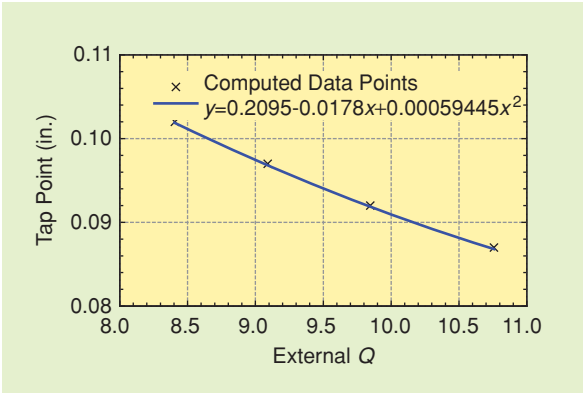

Figure 7. *Tap point in inches versus external Q for the resonator shown in Figure 6. As we can see from the polynomial coefficients, the curve is almost linear.*

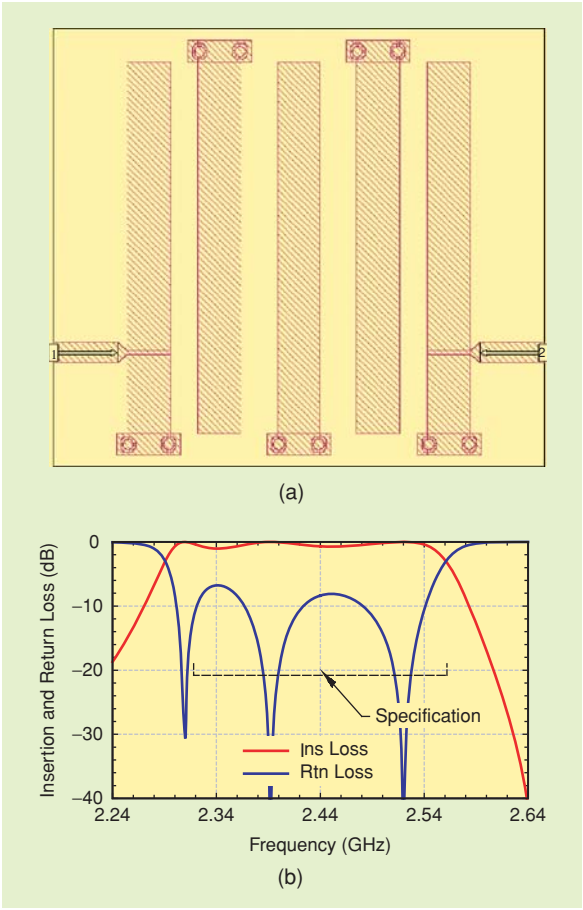

Figure 8. *(a) First-iteration filter layout: $S_1 = 33$ mil, $S_2 = 42$ mil, tap = 95 mil, and resonator lengths = 435 mil. The simulation box size is 572 by 512 by 150 mil. (b) Computed results. Sonnet* em *Ver. 11.52.*

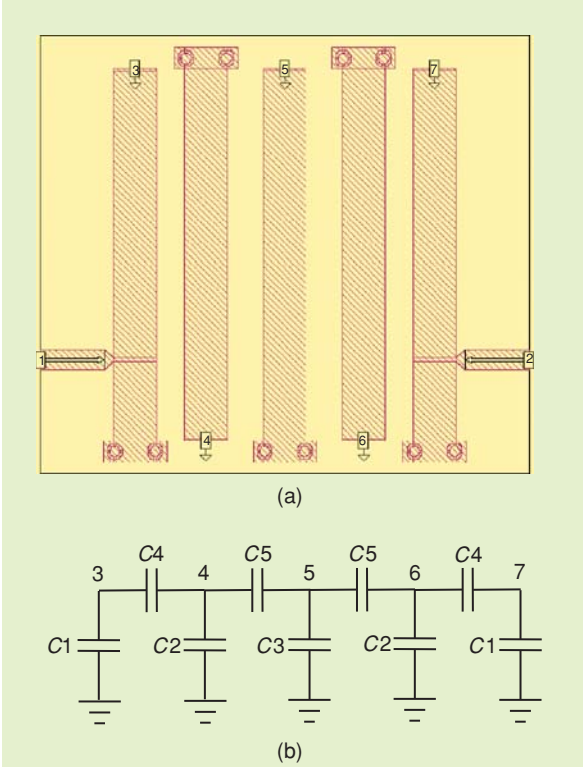

Figure 9. *(a) First-iteration geometry with added 50-Ω ports at the resonator open ends. (b) Array of tuning capacitors applied to the S-parameter data in a linear circuit simulator. Sonnet* em *Ver. 11.52.*

Although these first results may appear to be disappointing, they are predictable based on prior experience with this topology. The largest error is the tuning of the first and last resonators. It is well known in the filter design community that tapping has a major effect on resonator tuning, and the first and last resonators need to be considerably longer. However, it is not clear from these results what other corrections to resonator lengths or spacings may be needed. With some planar EM simulators, it would be tempting to parameterize this geometry and attempt to apply gradient optimization. Even if we consider symmetry, we have three resonator length variables, two resonator spacing variables, and the tap position. Just computing the gradients to begin the optimization process would take a considerable amount of time.

But if we apply port tuning and equal ripple optimization techniques [17] to the problem, we can rapidly determine the errors in this first iteration. Figure 9(a) shows the same geometry with 50-Ω ports added to the open ends of each resonator. In our circuit simulator, we can tune each resonator with a lumped capacitor to ground and tune each coupling with a capacitor between the resonator open ends. Figure 9(b) shows the array of tuning capacitors that is applied to the seven-port *S*-parameter data in a linear circuit simulator.

Figure 10 shows how the first-iteration results can be tuned to the exact equal ripple bandwidth and return loss level that we specified for this example. The tuning capacitor values are listed on the plot. To shift the return loss level, we would move the tap points up or down. As we can see, the largest correction has been applied to the first and last resonator tunings. We can go back to

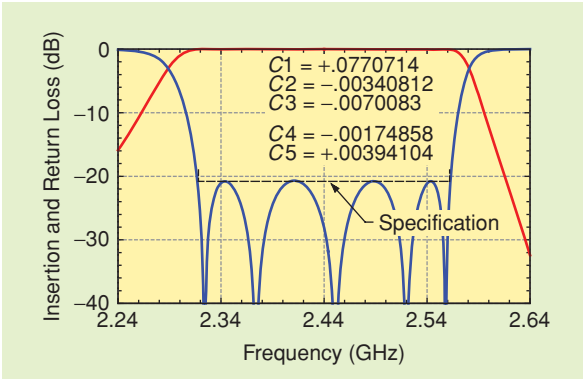

Figure 10. *First-iteration filter tuned to the exact equal ripple response and the required tuning capacitor values. The largest error is the first and last resonator tuning. Units are pF.*

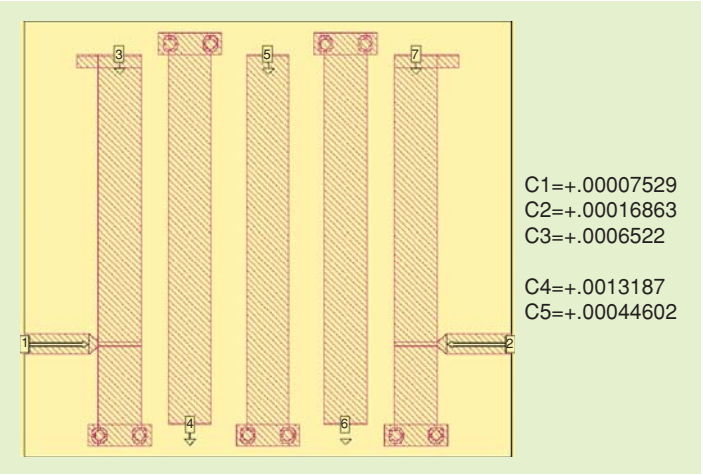

Figure 11. *Second-iteration geometry: $S_1 = 33$ mil, $S_2 = 41$ mil, with 16- by 19-mil "flags" added to the first and last resonators. Also shown are the tunings that bring it back to the exact equal ripple response. Units are pF. Sonnet* em *Ver. 11.52.*

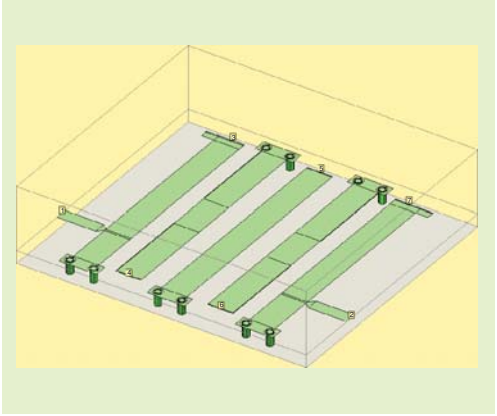

Figure 12. *Fourth-iteration geometry and final corrections that bring it back to exact equal ripple tuning. Metal has been removed from the outer edges of resonators two and four to reduce the first and last couplings. Units are pF. Sonnet* em *Ver. 11.52.*

the geometry in Figure 6 and estimate what amount of metal to add to realize the $C1$ tuning. The $C4$ and $C5$ tunings indicate that the first spacing should be bigger and the second spacing should be smaller. There are at least two ways to translate these tunings into physical dimensions. We can apply Dishal's methods to the tuned results in our circuit simulator. To extract the corrected $K_{1,2}$, we short circuit resonators three, four, and five and lightly couple to resonators one and two. We then extract the corrected $K_{1,2}$ from the resulting double-peaked S_{21} response. There is some potential error in this measurement introduced by the presence of the tap line. An alternate method would be to apply the correction capacitor to the geometry in Figure 3(c) (in our circuit simulator) and again compute the corrected $K_{1,2}$.

The corrected $K_{1,2}$ is .0863, which translates to a spacing of 33.2 mil, which we round down to 33 mil (no change). The corrected $K_{2,3}$ is .0658, which implies a spacing of 41.0 mil (change of -1 mil). The first and last resonator tunings are 16- by 19-mil "flags" of metal added to the open ends. The geometry of the second iteration is shown in Figure 11 along with the new tunings that bring it back to an exact equal ripple response.

All the resonator tuning errors are now quite small. The largest error is the first spacing, which is roughly the same as it was in the first iteration. With 1-mil resolution, we cannot set the spacing to exactly 33.2 mil. But we can remove some metal from the outer edges of the second and fourth resonators to effectively increase the spacing. We removed a strip of metal 1 mil wide and 88 mil long (20% of 435 mil) to approximate the 33.2-mil spacing. After simulating this new geometry and retuning, we found small tuning errors in resonators one, two, four, and five. The final correction to resonators one and two removed 1 by 7 mil of metal from the tuning flag. The final correction to resonators two and four removed 1 by 18 mil of metal from the resonator open end. No correction was made to resonator three. The tap position was never changed from the first iteration value of 95 mil. The geometry and tunings for iteration number four are shown in Figure 12.

Figure 13 shows the final filter simulation with and without tunings. At this point, the simulation is probably more precise than our knowledge of the exact substrate thickness and dielectric constant. There will also be manufacturing errors, which include etch tolerance and errors in registration between the metal pattern and the vias.

All the EM simulations of the complete filter have been lossless up to this point. This is both to save time (lossless simulations run much faster) and because the error function used in the equal ripple optimization assumes a lossless network. We can do one final simulation of the complete filter with loss included (Figure 14) to check the insertion loss across the passband, to

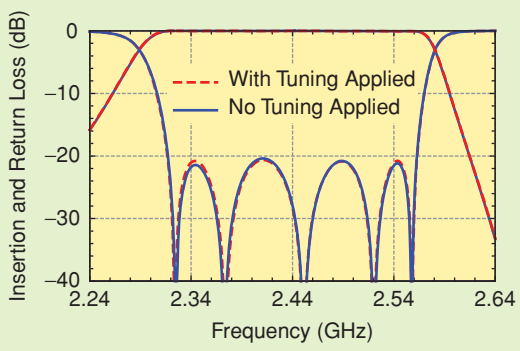

Figure 13. *Fourth-iteration filter simulation with and without final equal ripple tunings.*

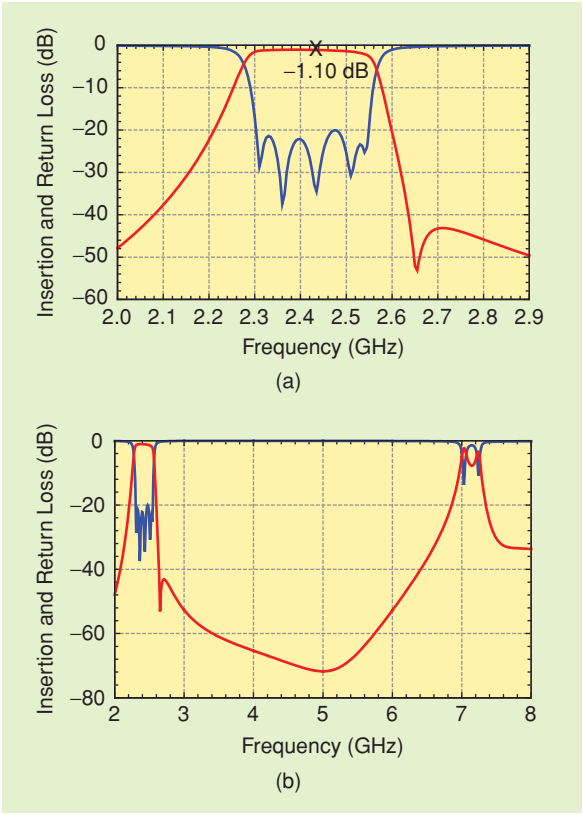

Figure 14. *Analysis of the fourth-iteration filter with loss and no tuning corrections. The midband loss is consistent with our earlier prediction based on the computed unloaded Q. The spurious passband at roughly $3f_0$ is consistent with interdigital filter theory.*

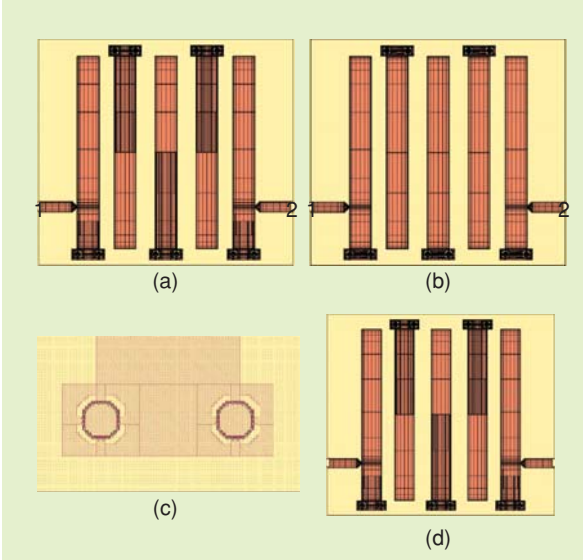

Figure 15. *Meshing the first-iteration filter. (a) Mesh generated using the via detail in (c). The meshing of the resonators is not as uniform as we would like. (b) Mesh generated using the via detail in (d). The meshing on the resonators is now more uniform and of lower density. The simulation time for (a) is roughly twice as long as (b) with no measurable difference in accuracy. Sonnet* em *Ver. 11.52.*

check the rejection levels we have achieved at key points in the stopband, and to look for spurious responses in the stopband.

The midband loss is consistent with our earlier prediction based on the computed unloaded *Q*. Note the asymmetry in the stopband skirts and the transmission zero on the high side of the passband which are typical for microstrip interdigital filters. The transmission zero causes the time delay to peak up at the upper band edge and, hence, the loss increases more rapidly at the upper band edge compared to the lower band edge. The spurious response at roughly $3f_0$ is typical for interdigital filters.

Method of Moments Mesh Control

Before we discuss the measured results, we should make a few comments about mesh control in the method of moments (MoM) simulations. MoM field solvers subdivide our planar metal patterns into a "mesh" of smaller units called cells or subsections and solve for the RF currents on each smaller unit. Theoretically, a finer and finer mesh will give us better and better accuracy. However, simulation time is roughly proportional to the size of the mesh cubed, which places a practical limit on mesh size. Ideally, we want just enough mesh in just the right places to generate a solution that is accurate enough for our design task. So when we study the mesh generated by the software, we are interested in both accuracy and efficiency.

Some readers may have noticed that each resonator in the filter is not drawn as a single closed polygon. We typically draw each resonator using a combination of polygons in order to control the meshing. Figure 15(a) shows the mesh for the first-iteration filter. Figure 15(c) shows how the via regions were drawn in this version. Note that there are regions on each resonator with a higher-density mesh. The extra meshing is caused by the via polygons (and their vertices) that border the resonator polygon. Figure 15(b) shows the same first-iteration filter, but with the via regions drawn in a different way. Again, Figure 15(d) shows the via region detail, which now has a single polygon bordering the resonator polygon. When we change how we draw the via region detail, the software generates a more uniform, lower-density mesh on the resonators. In both cases, we have placed the vias at the edges of the microstrip to capture the high current density found there [18].

These relatively minor changes in how the geometry is described by the user to the software result in large changes in mesh size, required memory, and simulation time. The mesh in Figure 15(a) has 12,346 subsections, requires 599 MB of RAM, and solves in 73 min (five frequency points). The mesh in Figure 15(b) has 9,755 subsections, requires 381 MB of RAM, and solves in 37 min (five frequency points). The computed *S*-parameters for the two meshes are virtually identical. Again, both

meshes are accurate, but with some thought and experimentation we can make a more efficient mesh. Of course, mesh efficiency becomes more important for higher-order filters or for more complicated topologies like diplexers or triplexers.

Experimental Results

The measured versus modeled results for our example filter are shown in Figure 16. A sample of four as-built filter substrates were measured with very similar results. The test fixture is a waveguide channel 572 mil long by 522 mil wide by 150 mil high. Note that the test fixture channel is 10 mil wider than our field solver simulation box. The measured equal ripple bandwidth is 253 MHz, which is 3.7% from our goal. Bandwidth was measured at the 20.8-dB return loss points. The measured center frequency is 2.422 GHz, which is 0.7% from the goal. The average insertion loss of the four filters at 2.44 GHz is 1.21 dB, which includes the SMA to microstrip launchers.

Note that the predicted depth and position of the high-side transmission zero is quite good. It is very difficult to consistently predict the location and depth of this transmission zero with a combination of analytical models in a circuit simulator. However, the full field solver model includes all the physics of the filter and the cutoff

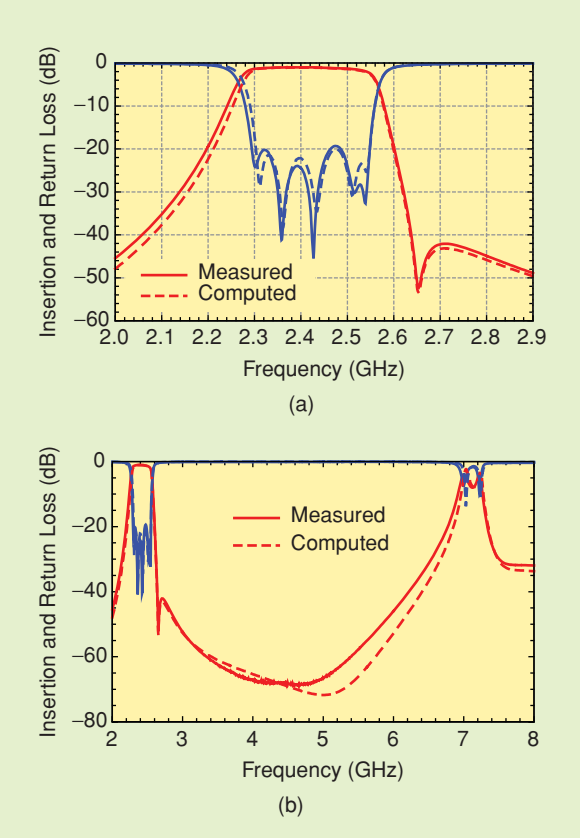

Figure 16. *Measured versus computed results for our example filter. Four substrates were measured with very similar results. The discrepancy deep in the stopband may be due to the test fixture.*

An EM-based filter prototype potentially captures all the physics of the real hardware and includes second-order effects that may be impossible to describe using analytical models.

waveguide channel and will consistently predict the true performance. The microstrip interdigital does not exhibit the $2f_0$ spurious response we often see in three-dimensional (3-D) transverse electromagnetic (TEM) interdigital filters and in microstrip edge-coupled filters.

Figure 17 shows the measured performance with the housing cover on and with the cover off. Note the significant bandwidth expansion with the cover off and how the bandwidth shift appears only on the low side of the passband. Similar behavior has been observed with microstrip edge-coupled filters in a narrow channel. This again emphasizes the strong interaction between the filter and the waveguide channel [15].

Although we have not done a thorough error analysis on these results, we can make a few observations. We can measure substrate thickness, but in general we do not know the exact relative dielectric constant of our substrate. The largest error is in the measured bandwidth, and there are at least three potential sources for this error. The first could be errors in the computed couplings in the MoM simulation. It is possible that the mesh is not sampling the fields at a high-enough rate along the length of the resonators. We can explore this possibility by forcing a finer mesh and recomputing. The second could be etch tolerance errors in the fabricated filters, which calls for careful measurement of the fabricated parts. And the third could be the 2% discrepancy in the width of the waveguide channel between the field-solver simulation and the test fixture.

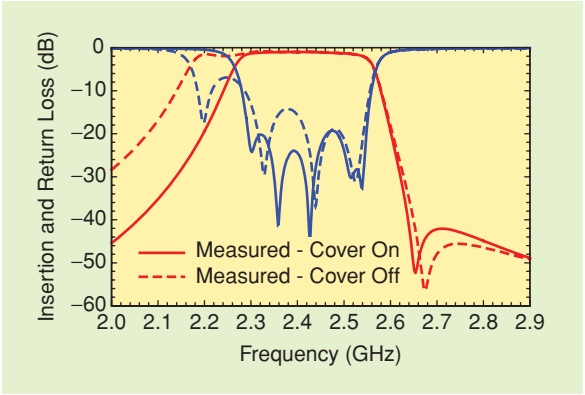

Figure 17. *Measured filter performance with the housing cover on and with the cover off. Note the significant shift in the filter bandwidth that appears only on the low side of the passband.*

A bandpass filter specification generally includes the desired center frequency, percentage bandwidth, maximum insertion loss in the passband, and several required rejection levels in the stopbands.

Conclusions

Dishal's design method for narrow-band filters offers a very simple and intuitive approach that can be applied to many different filter technologies and topologies. Using a field solver to generate the K and Q_{ex} design curves is very efficient and potentially more accurate compared to the older experimental method. With the addition of port-tuned EM models to the design flow, we can go one step beyond Dishal's original concept and build any number of virtual filter prototypes on the computer before we build any real hardware. When we tune the multiport S-parameter data from the virtual prototype to the desired exact equal ripple response, the tunings we have applied provide a very clear indication of the magnitude and direction of the needed corrections. The virtual prototype also predicts the exact shape of the filter skirts and the spurious responses in the stopband, which the original Dishal method could not do until the first hardware was built.

The port-tuning method is also very efficient in terms of compute time. We only solve the complete field solver project a few times and derive any gradient information we need from the tunings we apply in the circuit simulator. We can also avoid a lot of overshoot and undershoot in our corrections by addressing only one or two of the largest errors at each iteration. A more subtle advantage of the port-tuning method is in the number of frequencies we need to compute. The 50-Ω ports on the resonators completely detune the filter and greatly reduce the Q of the structure. Under these conditions, the computed S-parameters vary quite slowly across the passband of the filter. Only three frequencies that bracket the filter passband are needed from the field solver for each design iteration. As few as five frequencies can also provide data well into the stopbands. Thus, a very small compute farm of three to five nodes could significantly impact the design cycle time.

Although we have used a microstrip example here, the concepts we have presented apply equally well to cavity combline, interdigital, waveguide, and even dielectric resonator filters. For these types of filters we would typically use a finite element method (FEM) simulator rather than the MoM simulator used here. In [17], we reported the results for a cavity combline triplexer with cross-couplings in two of the three channels.

Finally, the flexibility of this design flow helps us overcome the limitations of fixed-grid, closed-box MoM simulators [19]. The port-tuned network gives very intuitive feedback on the corrections that need to be made. An experienced designer can then use engineering judgment and creativity to find adjustments that work within the limits of the geometrical resolution used in the EM simulation. In most cases, we can avoid high resolution (0.1 mil or .0025 mm) adjustments to the geometry that would force us to use a finer grid and dramatically increase simulation time.

References

[1] M. Dishal, "Alignment and adjustment of synchronously tuned multiple-resonant-circuit filters," *Proc. IRE*, vol. 39, pp. 1448–1455, Nov. 1951.

[2] M. Dishal, "A simple design procedure for small percentage bandwidth round-rod interdigital filters," *IEEE Trans. Microwave Theory Tech.*, vol. MTT-13, pp. 696–698, Sept. 1965.

[3] J.S. Wong, "Microstrip tapped-line filter design," *IEEE Trans. Microwave Theory Tech.*, vol. MTT-27, pp. 44–50, Jan. 1979.

[4] K. Puglia, "A general design procedure for bandpass filters derived from lowpass prototype elements: Part I," *Microwave J.*, vol. 43, no. 12, pp. 22–38, Dec. 2000.

[5] K. Puglia, "A general design procedure for bandpass filters derived from lowpass prototytpe elements: Part II," *Microwave J.*, vol. 44, no. 1, pp. 114–136, Jan. 2001.

[6] R. Rhea, "EM enables classic filter technique," *Microwave J.*, vol. 50, no. 2, pp. 138–146, Feb. 2007.

[7] J.G. Hong and M.J. Lancaster, *Microstrip Filters for RF/Microwave Applications*. New York: Wiley, 2001.

[8] D.G. Swanson, Jr. and R.J. Wenzel, "Fast analysis and optimization of combline filters using FEM," in *IEEE MTT-S Int. Microwave Symp. Dig.*, Phoenix, AZ, vol. 2, pp. 1159–1162, May 20–25, 2001.

[9] R.J. Wenzel and D.G. Swanson, Jr. "Observations on the stopband performance of tapped line filters," in *IEEE MTT-S Int. Microwave Symp. Dig.*, Phoenix, AZ, vol. 3, pp. 1619–1671, May 20–25, 2001.

[10] G.L. Matthaei, L. Young, and E.M.T. Jones, *Microwave Filters, Impedance-Matching Networks and Coupling Structures*. New York: McGraw-Hill, pp. 85–95, 1964.

[11] L. Weinberg, *Network Analysis and Synthesis*. New York: McGraw-Hill, p. 519, 1962.

[12] D.G. Swanson, Jr. and W.J.R. Hoefer, *Microwave Circuit Modeling Using Electromagnetic Field Simulation*. Dedham, MA: Artech House, pp. 378–384, 2003.

[13] MCPL Model, Ansoft Designer, Ansoft Corp., Pittsburg, PA. [Online]. Available: http://www.ansoft.com

[14] MMICTL Model, LINMIC Design Suite, AC Microwave GmbH, Aachen, Germany. [Online]. Available: http://www.linmic.com

[15] G.L. Matthaei, J.C. Rautio, and B.A. Willemsen, "Concerning the influence of housing dimensions on the response and design of microstrip filters with parallel-line couplings," *IEEE Trans. Microwave Theory Tech.*, vol. MTT-48, pp. 1361–1368, Aug. 2000.

[16] Sonnet *em*, Sonnet Software, North Syracuse, NY. [Online]. Available: http://www.sonnetusa.com

[17] D. Swanson and G. Macchiarella, "Microwave filter design by synthesis and optimization," *IEEE Microwave Mag.*, vol. 8, no. 2, pp. 55–69, Apr. 2007.

[18] D.G. Swanson, Jr., "Grounding microstrip lines with via holes," *IEEE Trans. Microwave Theory Tech.*, vol. MTT-40, pp. 1719–1721, Aug. 1992.

[19] D.G. Swanson, Jr., and W.J.R. Hoefer, *Microwave Circuit Modeling Using Electromagnetic Field Simulation*. Dedham, MA: Artech House, 2003, Chapter 5.